Nonequilibrium process of self-gravitating N-body systems and quasi-equilibrium structure using normalized q-expectation values for Tsallis' generalized entropy

doi: 10.1088/1742-6596/201/1/012009

Nonequilibrium process of self-gravitating N-body systems and quasi-equilibrium structure using normalized q-expectation values for Tsallis' generalized entropy

Nobuyoshi Komatsu[1], **Shigeo Kimura**[2], **Takahiro Kiwata**[1]

[1] Department of Mechanical Systems Engineering, Kanazawa University, Kakuma-machi, Kanazawa, Ishikawa 920-1192, Japan

[2] The Institute of Nature and Environmental Technology, Kanazawa University, Kakuma-machi, Kanazawa, Ishikawa 920-1192, Japan

E-mail: komatsu@t.kanazawa-u.ac.jp

Abstract. To clarify the nonequilibrium processes of self-gravitating systems, we examine a system enclosed in a spherical container with reflecting walls, by N-body simulations. To simulate nonequilibrium processes, we consider loss of energy through the reflecting wall, i.e., a particle reflected at a non-adiabatic wall is cooled to mimic energy loss. We also consider quasi-equilibrium structures of stellar polytropes to compare with the nonequilibrium process, where the quasi-equilibrium structure is obtained from an extremum-state of Tsallis' entropy. Consequently, we numerically show that, with increasing cooling rates, the dependence of the temperature on energy, i.e., the ε–$\hat{T}$ curve, varies from that of microcanonical ensembles (or isothermal spheres) to a common curve. The common curve appearing in the nonequilibrium process agrees well with an ε–$\hat{T}$ curve for a quasi-equilibrium structure of the stellar polytrope, especially for the polytrope index $n \sim 5$. In fact, for $n > 5$, the stellar polytrope within an adiabatic wall exhibits gravothermal instability [Taruya, Sakagami, Physica A, 322 (2003) 285]. The present study indicates that the stellar polytrope with $n \sim 5$ likely plays an important role in quasi-attractors of the nonequilibrium process in self-gravitating systems with non-adiabatic walls.

1. Introduction

Self-gravitating or long-range attractive interacting systems exhibit several peculiar features, such as negative specific heat and nonequilibrium non-extensive statistical mechanics. For example, negative specific heat plays an important role in astrophysical phenomena, especially in the gravothermal catastrophe of globular clusters [1, 2]. In such systems, standard Boltzmann–Gibbs statistics are not valid because of the existence of long-range potentials. Therefore, non-extensive statistics have been investigated based on Tsallis' generalized entropy [3, 4], by Plastino et al. [5], Abe [6], Chavanis [7] and many other researchers (see e.g. Ref. [4] and references therein).

Recently, from an astrophysical viewpoint, Taruya and Sakagami [8, 9, 10, 11, 12] have elegantly shown that an extremum-state of Tsallis' entropy, i.e., a *stellar polytrope*, has a consistent thermodynamic structure, which implies a thermodynamic instability because of

the negative specific heat. They focused on quasi-equilibrium structures of stellar polytropic systems and examined a system enclosed in a spherical container with reflecting walls. This result suggests that the stellar quasi-equilibrium distribution can be described by the stellar polytrope and that the stellar polytropic distribution is expected to be a quasi-attractor of self-gravitating systems. The earlier studies mainly investigated microcanonical ensembles, since a system within an adiabatic wall or the so-called *Antonov problem* [1, 2, 13, 14] is essential for studying self-gravitating systems such as globular clusters.

In fact, from the viewpoint of thermodynamic properties, the influence of energy loss or variation in energy (e.g., the evaporation of stars from globular clusters or radiation loss) has not been examined in detail, with only a few studies [15] considering this influence. Thus it is not yet clear whether the stellar polytrope can be applied to a nonequilibrium process with energy loss and it is therefore important to investigate numerically the thermodynamic properties of the nonequilibrium process with energy loss. In this context, we examine a self-gravitating system enclosed in a spherical container with reflecting walls, by N-body simulations. In this study, a particle reflected at a non-adiabatic wall is cooled to mimic energy loss for nonequilibrium processes. Through this investigation, we attempt to apply the stellar polytrope to the nonequilibrium process with a non-adiabatic wall.

The present paper is organized as follows. In Sec. 2, we give a brief review of numerical techniques for simulating a self-gravitating system enclosed in a spherical container with non-adiabatic walls. In Sec. 3, we briefly review a quasi-equilibrium structure of stellar polytropes calculated from an extremum-state of Tsallis' entropy. In Sec. 4, we present the simulation results and examine the nonequilibrium process with non-adiabatic walls, by a comparison with the stellar polytrope. Finally, we present our conclusions. In this paper, the results shown in Ref. [16] are reconsidered and discussed from the viewpoint of an application of Tsallis' entropy.

2. N-body simulations

We consider a simple system consisting of N point-particles enclosed in a spherical container of radius R with reflecting walls, as shown in Fig. 1. To simulate nonequilibrium processes, we consider the loss of energy through the reflecting wall, i.e., a particle reflected at a non-adiabatic wall is cooled to mimic energy loss. In this section, we briefly review a method to simulate the nonequilibrium process, according to Ref. [16].

To simulate a self-gravitating N-body system, we integrate the set of classical equations of motion for the particles interacting through the Plummer softened potential,

$$\Phi = -\frac{1}{\sqrt{r^2 + r_0^2}}, \tag{1}$$

where r and r_0 represent the distance between particles and the softening parameter, respectively

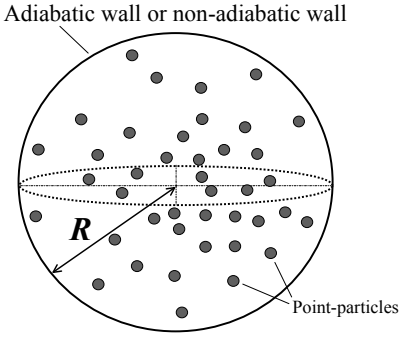

Figure 1. Setup for the N-body simulation. We consider a simple self-gravitating system consisting of N point-particles enclosed in a spherical container of radius R with adiabatic or non-adiabatic walls.

[17, 18, 19]. The total energy E of the self-gravitating N-body system is defined as

$$E = E_{\rm KE} + E_{\rm PE} = \sum_{i}^{N} \frac{m_i v_i^2}{2} - \sum_{i<j}^{N} \frac{G m_i m_j}{\sqrt{r_{ij}^2 + r_0^2}}, \tag{2}$$

where $E_{\rm KE}$, $E_{\rm PE}$ and m_i represent kinetic energy, potential energy and the mass of the i-th point-particle, respectively. G, v_i and r_{ij} represent the gravitational constant, the speed of the i-th particle and the distance between the i-th and j-th particles, respectively. The mass of each particle is set to be m. Applying traditional conventions for self-gravitating systems, the total rescaled energy ε is defined as

$$\varepsilon = \varepsilon_{\rm KE} + \varepsilon_{\rm PE} = E\frac{R}{GM^2} = E\frac{R}{G(mN)^2}, \tag{3}$$

where M, $\varepsilon_{\rm KE}$ and $\varepsilon_{\rm PE}$ represent the total mass, rescaled kinetic and potential energies, respectively. In this study, the unit of time is $\sqrt{R^3/(Gm)}$. The units are set to be $G = R = m = 1$, to ensure generality of the system. In our units, the temperature $\hat{T}$ of the system is given by

$$\hat{T} = \frac{2}{3k_{\rm B}}\varepsilon_{\rm KE} = \frac{2}{3}\varepsilon_{\rm KE}, \tag{4}$$

assuming that the kinetic energy corresponds to the temperature and that Boltzmann's constant $k_{\rm B}$ is 1.

In this study, we consider a small system consisting of $N = 250$ point-particles in a spherical container of radius $R = 1$. For simulating the N-body system, the set of equations of motion is integrated using Verlet's algorithm. To maintain the accuracy of our simulations, the time step Δt is selected as 10^{-5}, based on a simulation with several different time-steps [17]. Through the present simulations, all interparticle forces are calculated directly at each time step Δt. In this paper, all the numerical results are averaged over 30 simulations with identically prepared initial setups, to observe an averaged behavior of the system.

To mimic a spherical adiabatic wall for microcanonical ensembles, the radial component of the velocity of a particle is reversed when it reaches the wall [17]. Accordingly, the velocity speed $|\boldsymbol{v}_i|$ of the particle is conserved through the reflection. In contrast, to mimic a spherical non-adiabatic wall for nonequilibrium processes, the velocity after the reflection is reduced as

$$\boldsymbol{v}_i^{(\rm reflected)} = (1-\gamma)\boldsymbol{v}_i, \tag{5}$$

where γ is a velocity reduction rate or a cooling rate [16]. That is, a non-adiabatic wall is employed to simulate energy loss by reflecting walls. The cooling rate γ is varied from 0.001 to 0.8, to investigate the influence of the non-adiabatic wall. Note that $\gamma = 0$ corresponds to the adiabatic wall for a microcanonical ensemble. We have checked the total angular momentum through our simulations and confirmed that the variation in total angular momentum is sufficiently small to avoid a phase transition of the system.

For the Plummer softened potential, the softening parameter r_0 is set to be $0.005R$. Accordingly, the collapse and explosion energies for the system with an adiabatic wall [18] are $\varepsilon_{coll} \approx -0.339$ and $\varepsilon_{expl} \approx 0.267$, respectively. In such self-gravitating systems, the crossing time τ_c and the relaxation time τ_r are evaluated as $\tau_c \approx 1/\sqrt{G\rho} = 1/\sqrt{\rho}$ and $\tau_r \approx (0.1N/\ln N)\tau_c$, respectively, where ρ represents the density of the system [13]. In our units, the crossing and relaxation times are $\tau_c \approx 0.1$ and $\tau_r \approx 0.6$, respectively, assuming a uniform density profile. The collapse time of the present system is approximately 600, since the collapse time in a system with $N = 125$–250 particles and $r_0 = 0.005R$ is approximately $\sim 10^3\tau_r$ [19].

For the initial setup, we prepared a self-gravitating system at an approximate virial equilibrium state, by means of 30 microcanonical ensemble simulations in which each simulation time is 10 time units [16]. In the present simulation, the initial total energy ε_0 is set to be 0.5, which is higher than the explosion energy $\varepsilon_{expl} \approx 0.267$. Note that the initial total momentum and initial total angular momentum are set to be 0. To check the system, we examined density profiles and found that the density profile is slightly nonuniform at $\varepsilon_0 = 0.5$, which is generally considered as the uniform state. We also confirmed that the system is in an approximate virial equilibrium state using the virial ratio. Therefore, in our simulations, we employ the above system as the initial setup. The initial energies are $\varepsilon_0 = 0.5000 \pm 0.0096$, $\varepsilon_{\mathrm{KE}_0} = 1.1206 \pm 0.0109$ and $\varepsilon_{\mathrm{PE}_0} = -0.6206 \pm 0.0076$, where the errors indicate the 68% confidence level in terms of the normal error distribution. We have confirmed that our main results do not greatly depend on the initial total energy, e.g., $\varepsilon_0 = 0.3$.

Using the above initial setup, a simulation for a system with a non-adiabatic wall was carried out with various cooling rates γ. For $\gamma = 0.001$, 0.01, 0.1 and 0.2–0.8, the simulation time is $t = 100$, 18, 4 and 2, respectively. Accordingly, our simulation time should be shorter than the collapse time of the present system, ~ 600; that is, we examine an early relaxation process before the collapse. As for $\gamma = 0$, a microcanonical ensemble simulation is carried out.

3. Stellar polytrope

Taruya and Sakagami [8, 9, 10, 11, 12] have shown that the extremum-state of Tsallis' entropy, i.e., the *stellar polytrope*, has a consistent thermodynamic structure, which implies thermodynamic instability due to a negative specific heat. They found that the stellar polytropic distribution should be a quasi-attractor of self-gravitating systems. We expect that the quasi-equilibrium structure of the stellar polytrope should be related to a nonequilibrium process appearing in the self-gravitating system with a non-adiabatic wall. Therefore, we briefly review the stellar polytrope calculated from an extremum-state of Tsallis' entropy, according to the works of Taruya and Sakagami [11, 12].

3.1. Tsallis' entropy and stellar polytrope

In the new framework of Tsallis' non-extensive thermo statistics, all the macroscopic observables of quasi-equilibrium systems should be characterized by escort distributions, although the escort distributions themselves should not be fundamental [11, 12]. In fact, we can find a more fundamental probability function $p(\boldsymbol{x}, \boldsymbol{v})$ that quantifies the phase-space structure, where $(\boldsymbol{x}, \boldsymbol{v})$ represents 6-dimensional phase-space. Note that the phase-space measure is defined as $\mathrm{d}^6\boldsymbol{\tau} \equiv \mathrm{d}^3\boldsymbol{x}\mathrm{d}^3\boldsymbol{v}/h^3$, where $h^3 \equiv (l_0 v_0)^3$ represents the phase-space element with the unit of length l_0 and the unit of velocity v_0.

Using the fundamental probability function $p(\boldsymbol{x}, \boldsymbol{v})$, the escort distribution is defined as

$$P_q(\boldsymbol{x}, \boldsymbol{v}) = \frac{\{p(\boldsymbol{x}, \boldsymbol{v})\}^q}{\int \mathrm{d}^6\boldsymbol{\tau}\{p(\boldsymbol{x}, \boldsymbol{v})\}^q}, \tag{6}$$

and the macroscopic observables expressed as normalized q-expectation values are given by

$$\langle O_i \rangle_q = \int \mathrm{d}^6\boldsymbol{\tau}\{O_i P_q(\boldsymbol{x}, \boldsymbol{v})\}, \tag{7}$$

where the normalization condition for $p(\boldsymbol{x}, \boldsymbol{v})$ is given as

$$\int \mathrm{d}^6\boldsymbol{\tau}\{p(\boldsymbol{x}, \boldsymbol{v})\} = 1. \tag{8}$$

Tsallis' generalized entropy is given as

$$S_q = -\frac{1}{q-1}\int \mathrm{d}^6\boldsymbol{\tau}[\{p(\boldsymbol{x},\boldsymbol{v})\}^q - p(\boldsymbol{x},\boldsymbol{v})]. \tag{9}$$

Through an extremum-state of Tsallis' entropy, i.e., solving the variational problem, Taruya and Sakagami have shown that the polytropic relation can be given as

$$P(r) = K_n\{\rho(r)\}^{1+1/n}, \tag{10}$$

where K_n, $P(r)$ and $\rho(r)$ are the dimensional constant, the isotropic pressure and the density at radius r, respectively [11, 12]. The polytrope index n is given by

$$n = \frac{1}{1-q} + \frac{1}{2}. \tag{11}$$

3.2. Emden solutions and thermodynamic properties of the stellar polytrope

In this section, we focus on a spherically symmetric system with polytrope index $n > 3/2$, in which the equilibrium distribution is at least *dynamically* stable [13]. In such situations, the stellar equilibrium distribution should be characterized by the so-called *Emden solutions*, and all the physical quantities should be discussed using the homology invariant variables [12]. For example, Chavanis examined the gravitational instability of isothermal and polytropic spheres in detail, using the Milne variables [7, 22, 23]. Note that we consider here a quasi-equilibrium structure of the stellar polytropic system with pure gravitational potentials [11, 12].

The equations for the hydrostatic equilibrium of self-gravitating systems [11, 12] are given by

$$\frac{\mathrm{d}P(r)}{\mathrm{d}r} = -\frac{Gm(r)}{r^2}\rho(r), \tag{12}$$

$$\frac{\mathrm{d}m(r)}{\mathrm{d}r} = 4\pi\rho(r)r^2, \tag{13}$$

where $m(r)$ represents the mass evaluated at radius r. The dimensionless quantities, i.e., θ and ξ, are introduced as

$$\rho = \rho_c[\theta(\xi)]^n, r = \left\{\frac{(n+1)P_c}{4\pi G{\rho_c}^2}\right\}^{1/2}\xi, \tag{14}$$

where ρ_c and P_c are the density and pressure at the center of the spherical container, respectively. Then, the ordinary differential equation for the hydrostatic equilibrium is given as

$$\theta'' + \frac{2}{\xi}\theta' + \theta^n = 0, \tag{15}$$

and the boundary conditions are set to be

$$\theta(0) = 1, \theta'(0) = 0, \tag{16}$$

where the prime represents the derivative with respect to ξ, i.e., $\mathrm{d}/\mathrm{d}\xi$. Solutions of Eq. (15) with (16), i.e., Emden solutions, are calculated numerically using, for example, Runge–Kutta methods. This is because the solution cannot be solved analytically, except for the polytrope indices, $n = 0$, 1 and 5.

To characterize the equilibrium properties of the Emden solution [11, 12], homology invariants are defined as

$$u \equiv \frac{\mathrm{d}\ln m(r)}{\mathrm{d}\ln r} = \frac{4\pi r^3 \rho(r)}{m(r)} = -\frac{\xi\theta^n}{\theta'}, \tag{17}$$

$$v \equiv -\frac{\mathrm{d}\ln P(r)}{\mathrm{d}\ln r} = \frac{\rho(r)}{P(r)}\frac{Gm(r)}{r} = -(n+1)\frac{\xi\theta'}{\theta}. \tag{18}$$

In the following, we consider a quasi-equilibrium structure of the stellar polytropic system enclosed in a spherical container with adiabatic walls. Taruya and Sakagami have evaluated the total energy E of a confined stellar system in terms of the total mass M, the pressure P_e and density ρ_e at the boundary r_e. (They considered an extremum-state of Tsallis' entropy at a fixed mass and energy.) Moreover, they determined a plausible physical temperature T_{phys}, using the modified Clausius relation [11, 12]. Based on this analysis, as a function of the homology invariants at the wall, i.e., u_e and v_e, the dimensionless quantities for the total energy and inverse temperature are given by

$$\lambda \equiv -\frac{Er_e}{GM^2} = -\frac{1}{n-5}\left\{\frac{3}{2}\left(1-\frac{n+1}{v_e}\right)+(n-2)\frac{u_e}{v_e}\right\}, \tag{19}$$

$$\eta \equiv \frac{GM^2}{r_e T_{phys}} = \frac{(n-5)v_e}{n+1-2u_e-v_e}, \tag{20}$$

where r_e corresponds to R in the present study. For details, see Eqs. (37) and (42) in Ref. [11] or Eqs. (3.27) and (3.33) in Ref. [12].

In our units, the total rescaled energy and temperature can be given as

$$\varepsilon = -\lambda, \tag{21}$$

$$\hat{T} = 1/\eta. \tag{22}$$

To confirm the thermodynamic properties of the stellar polytrope, we observe the trajectories of the Emden solutions in the ε–$\hat{T}$ plane. As shown in Fig. 2, for higher energies, the temperature $\hat{T}$ decreases with decreasing total energy ε. Accordingly, the system behaves like an ideal gas with a positive specific heat, i.e., $d\varepsilon/d\hat{T} > 0$. In contrast, for lower energies, the temperature increases as the total energy decreases. In other words, the specific heat in this region is negative, i.e., $d\varepsilon/d\hat{T} < 0$. This is because the potential energy of the system is dominant in the lower energy

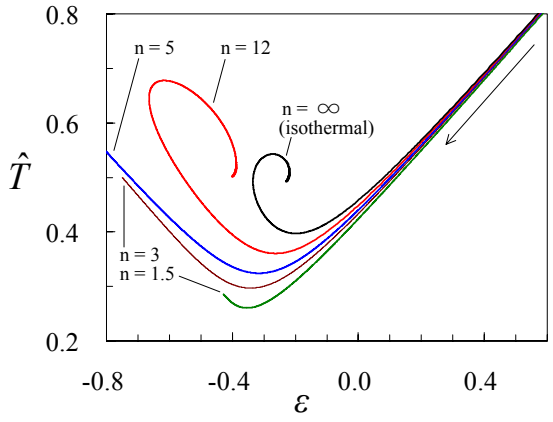

Figure 2. (Color online) Trajectories of Emden solutions in the ε–$\hat{T}$ plane. Each point along the trajectory represents an Emden solution evaluated at different radiuses r_e. Based on the boundary conditions, all the trajectories start from $(\varepsilon,\ \hat{T}) = (\infty,\ \infty)$ corresponding to the limit $r_e \to 0$. With increasing radius, the trajectories move as indicated by the arrow. The polytrope index $n = \infty$ corresponds to an isothermal sphere [16].

region. We now observe the influence of the polytrope index n. We find that the trajectories for $n > 5$ gradually change their direction and finally spiral around a fixed point, while the trajectories for $n < 5$ terminate suddenly because of the finite radius [11]. In fact, for $n > 5$, a stellar polytrope within an adiabatic wall exhibits gravothermal instability, as investigated by Taruya and Sakagami [11, 12].

4. Results

We first examine the nonequilibrium process with non-adiabatic walls by N-body simulations. For this, we observe typical time evolutions of the energies for $\gamma = 0.001$, 0.01, 0.1, 0.2, 0.3, 0.4 and 0.5. As shown in Fig. 3, the total energy ε decreases rapidly from the initial total energy of $\varepsilon_0 = 0.5$, due to the non-adiabatic wall. Hereafter we call the first stage the *rapid initial cooling stage* [20]. We can confirm that the behavior of each curve is consistent, especially during the rapid initial cooling stage. Similarly, the kinetic energy $\varepsilon_{\rm KE}$ decreases with γt during the rapid initial cooling stage. However, the kinetic energy gradually increases after this stage, while the total energy decreases, i.e., $d\varepsilon/d\varepsilon_{\rm KE}$ is negative. This indicates that an incidence of negative specific heat occurs, assuming that the kinetic energy corresponds to the temperature of the system [16].

For $\gamma = 0.3$, 0.4 and 0.5, the kinetic energy oscillates considerably during the rapid initial cooling stage, after which the amplitude of the oscillations decays. This is because, for larger cooling rates, the decrease in energy is too large to maintain the virial equilibrium state during the rapid initial cooling stage [16]. However, all the systems are in an approximate virial equilibrium state, except around the large oscillations and the rapid initial cooling stage. We have confirmed that the oscillation does not greatly depend on the average operation and the time step. The oscillation may disappear when the number of particles is large [21].

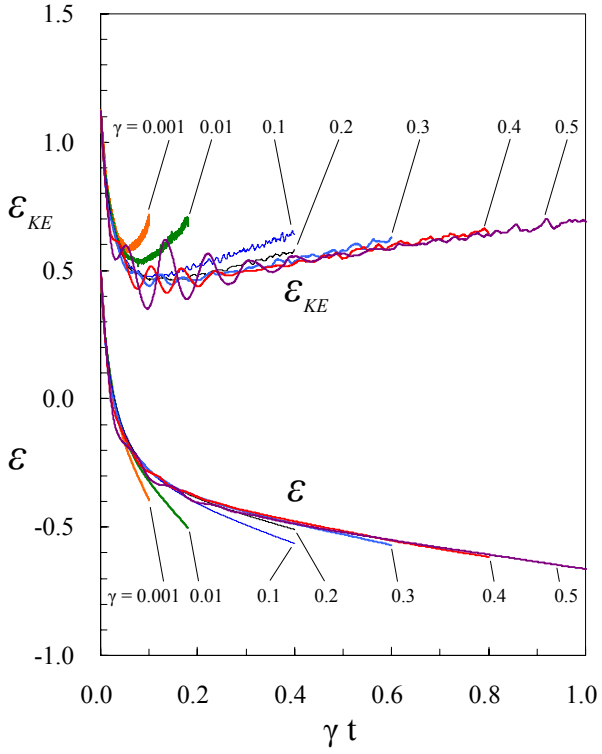

Figure 3. (Color online) Time evolutions of the total energy ε and kinetic energy $\varepsilon_{\rm KE}$, for various cooling rates γ. The horizontal axis represents the rescaled time γt. The results are averaged over 30 simulations with identically prepared initial setups [16].

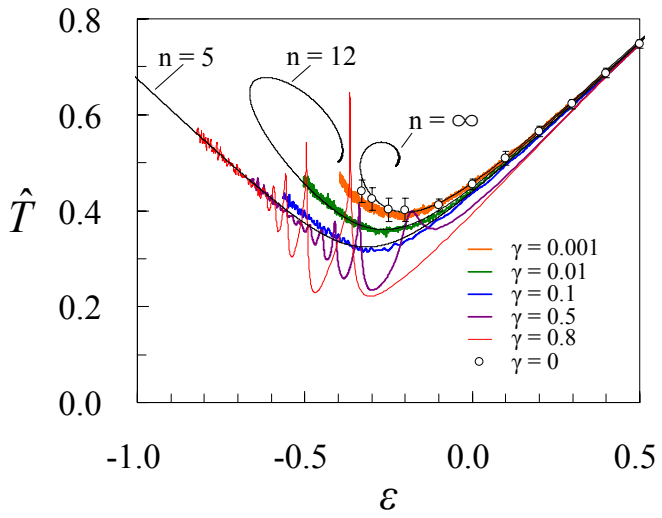

Figure 4. (Color online) Dependence of the temperature $\hat{T}$ on the total energy ε for various cooling rates γ and polytrope indices n. For $\gamma > 0$, the simulation starts from an initial total energy of $\varepsilon_0 = 0.5$. The open circles represent $\gamma = 0$, i.e., microcanonical ensemble simulations [16]. The trajectories of Emden solutions with $n = 5$, 12 and ∞ are re-plotted from Fig. 2.

Next, to examine the nonequilibrium processes of the self-gravitating system, we observe the dependence of the temperature $\hat{T}$ on the total energy ε for various cooling rates, as shown in Fig. 4. In this figure, we calculate the temperature $\hat{T}$ from the kinetic energy using Eq. (4). (The assumption that the kinetic energy corresponds to the temperature of the system is valid, since all the systems are in an approximate virial equilibrium state, except around the large oscillations and the rapid initial cooling stage [16].) Moreover, in Fig. 4, we re-plot the trajectories of the Emden solutions for the polytrope indices $n = 5$, 12 and ∞, to compare with the nonequilibrium process for various cooling rates. Note that a pure gravitational potential is used for the stellar polytrope, while the softening parameter is set to be $r_0 = 0.005R$ in our nonequilibrium simulations. Accordingly, we have to take into account the influence of the softening parameter, since it affects the dependence of the temperature on the total energy.

As shown in Fig. 4, our microcanonical ensemble simulations ($\gamma = 0$) are consistent with the isothermal sphere ($n = \infty$), except for a part of the spiral curve. The difference between $\gamma = 0$ and $n = \infty$ indicates the influence of the deviation from a pure gravitational potential. For $-0.2 \lessapprox \varepsilon$, the system behaves like an ideal gas with a positive specific heat, while the specific heat for $\varepsilon \lessapprox -0.2$ is negative [16]. To compare with the microcanonical ensemble, we examine a system with a small cooling rate, $\gamma = 0.001$. (The simulations for $\gamma > 0$ start from an initial total energy of $\varepsilon_0 = 0.5$.) As expected, the result for $\gamma = 0.001$ agrees well with the microcanonical ensemble ($\gamma = 0$), although the temperature for $\gamma = 0.001$ is slightly lower than that for $\gamma = 0$. We can confirm that a negative specific heat occurs not only in the microcanonical ensemble but also in certain nonequilibrium processes with a non-adiabatic wall.

Now, we investigate the influence of the cooling rate more closely. As shown in Fig. 4, for $-0.2 \lessapprox \varepsilon$, the curve further deviates from the microcanonical ensemble ($\gamma = 0$) with increasing cooling rate γ. In other words, the greater the cooling rate, the steeper the slope of the curve. For $\varepsilon \lessapprox -0.2$, or rather $\varepsilon \lessapprox \varepsilon_{coll}$, the temperature increases with decreasing total energy, excepting several large oscillations. (All the systems are in an approximate virial equilibrium state, except around the large oscillations and the rapid initial cooling stage.) Therefore, it is clearly demonstrated that a negative specific heat occurs in the system for various cooling rates. Moreover, each curve gradually shifts towards a certain common curve. However, the extent of the negative specific heat or $d\varepsilon/d\hat{T}$ does not greatly depend on the cooling rate. That is, with increasing cooling rate, the dependence of the temperature on energy, i.e., the ε–$\hat{T}$ curve, varies from the microcanonical ensemble to a common curve.

We expect that the tendency towards a common curve is related to a kind of quasi-attractor

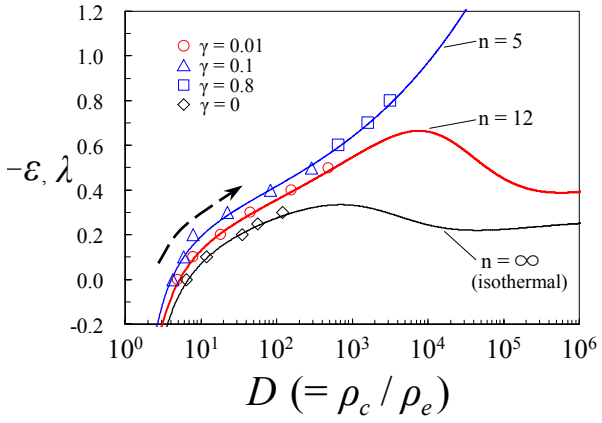

Figure 5. (Color online) Density contrast $D(=\rho_c/\rho_e)$ and the negative of the energy $\lambda(=-\varepsilon)$. The real lines represent the stellar polytropes with $n = 5$, 12 and ∞. The symbols represent the simulation results of the nonequilibrium process for various cooling rates γ. For $\gamma > 0$, the symbols represent evolutionary states; that is, the states for $\gamma > 0$ evolve as indicated by the arrow, as time progresses.

discussed in Ref. [8] by Taruya and Sakagami. (Note that the stellar polytrope examined by Taruya and Sakagami is assumed to be a quasi-equilibrium structure under the restriction of constant total energy, while the total energy is not fixed in the present nonequilibrium simulation.) Accordingly, we compare our nonequilibrium process with a quasi-equilibrium structure of stellar polytropes. We find that the common curve appearing in the nonequilibrium process agrees well with an ε–$\hat{T}$ curve for the polytrope index of $n = 5$. (The polytrope index of $n = 5$ corresponds to the appearance of gravothermal instability for a stellar polytrope within an adiabatic wall [11, 12].) This indicates that a quasi-equilibrium structure for a stellar polytrope with $n \sim 5$ should play an important role in quasi-attractors of the present nonequilibrium simulation. (We have confirmed that the tendency towards a common curve does not greatly depend on the softening parameter, e.g., $r_0 = 0.050R$. Of course, the deviation from the ε–$\hat{T}$ curve for $n = 5$ depends on the softening parameter.) Moreover, we found that the curve for $\gamma = 0.01$ agrees well with the curve for a polytrope index of $n = 12$, except for a part of the spiral curve.

As discussed above, the present nonequilibrium process is expected to be related to the stellar polytrope. To examine this more closely, we observe the relationship between the density contrast $D = \rho_c/\rho_e$ and the negative of the total energy $\lambda(=-\varepsilon)$, for various cooling rates γ and polytrope indices n. (Here ρ_c and ρ_e represent the densities at the center and wall, respectively. Based on the works of Taruya and Sakagami [11, 12], $\lambda(=-\varepsilon)$ is used in this discussion.) To obtain the density contrast for various cooling rates, the density profile calculated from the Emden solution is fitted with the corresponding density profile of our simulations, using Eq. (14). Based on the fitted curves, we evaluated the density contrast for various cooling rates. In Fig. 5, typical density contrasts are plotted except for large oscillations of the large cooling rates. Note that, for $\gamma > 0$, the symbols in the figure represent evolutionary states; that is, the states for $\gamma > 0$ evolve as indicated by the arrow, as time progresses.

As shown in Fig. 5, the results for $\gamma = 0$ ($\diamondsuit$) and $\gamma = 0.01$ ($\circ$) agree well with the D–λ curves for $n = \infty$ and $n = 12$, respectively. As expected, this is consistent with the result shown in Fig. 4. Similarly, the results for $\gamma = 0.1$ ($\triangle$) and $\gamma = 0.8$ ($\square$) agree well with the D–λ curve for $n = 5$. That is, the common curve appearing in $\gamma = 0.1$–0.8 is likely to be related to stellar polytrope with $n \sim 5$. Of course, the stellar polytrope is assumed to be a quasi-equilibrium structure under the restriction of constant total energy. However, these results indicate that the stellar polytrope calculated from Tsallis' entropy can be applied to the present nonequilibrium process with a non-adiabatic wall.

5. Conclusions

To clarify the nonequilibrium processes of self-gravitating systems, we examined a system enclosed in a spherical container with reflecting walls, by N-body simulations. For this, we investigated the nonequilibrium process numerically and compared it with a quasi-equilibrium structure of stellar polytropes, which is calculated from an extremum-state of Tsallis' generalized entropy. In our simulations, for microcanonical ensembles, the radial component of the velocity of a particle was reversed when it reached the wall. In contrast, for simulating a nonequilibrium process, we considered loss of energy through the reflecting wall, i.e., a particle reflected at a non-adiabatic wall was cooled to mimic energy loss. We have shown that, with increasing cooling rates, the dependence of the temperature on energy, i.e., the ε–$\hat{T}$ curve, varies from the microcanonical ensemble to a common curve. The common curve appearing in the nonequilibrium process is consistent with an ε–$\hat{T}$ curve for the polytrope index $n = 5$ corresponding to the appearance of gravothermal instability. This indicates that the quasi-equilibrium structure of stellar polytropes for $n \sim 5$ should play an important role in quasi-attractors of the nonequilibrium process appearing in a self-gravitating system with a non-adiabatic wall. The stellar polytrope considered here is assumed to be a quasi-equilibrium structure under the restriction of constant total energy. However, we found that the stellar polytrope calculated from Tsallis' entropy can be applied to the nonequilibrium process with a non-adiabatic wall. That is, the behavior of the present nonequilibrium process is likely to be related to the stellar polytrope.

We are grateful to Prof. M. Sakagami for valuable comments in the Kyoto RIMS workshop.

References

[1] Antonov V A 1962 Vestn. Leningrad Univ. **7** 135; *in Dynamics of Globular Clusters*, edited by Goodman J and Hut P 1985 *IAU Symposium* No. 113 (Reidel, Dordrecht)
[2] Lynden-Bell D and Wood R 1968 *Mon. Not. R. Astron. Soc.* **138** 495
[3] Tsallis C 1988 *J. Stat. Phys.* **52** 479
[4] Tsallis C 2009 *Introduction to Nonextensive Statistical Mechanics: Approaching a Complex World* (Springer)
[5] Plastino A and Plastino A R 1993 *Phys. Lett. A* **174** 384
[6] Abe S 1999 *Phys. Lett. A* **263** 424
[7] Chavanis P H 2002 *Astron. Astrophys.* **386** 732
[8] Taruya A and Sakagami M 2003 *Phys. Rev. Lett.* **90** 181101
[9] Taruya A and Sakagami M 2005 *Mon. Not. R. Astron. Soc.* **364** 990
[10] Taruya A and Sakagami M 2002 *Physica (Amsterdam)* **307A** 185; 2003 *Physica (Amsterdam)* **318A** 387
[11] Taruya A and Sakagami M 2003 *Physica (Amsterdam)* **322A** 285
[12] Sakagami M and Taruya A 2004 *Continuum Mech. Thermodyn.* **16** 279
[13] Binney J and Tremaine S 1987 *Galactic Dynamics* (Princeton University Press, Princeton)
[14] Padmanabhan T 1990 *Phys. Rep.* **188** 285
[15] Posch H A and Thirring W 2005 *Phys. Rev. Lett.* **95** 251101
[16] Komatsu N, Kimura S and Kiwata T 2009 *Phys. Rev. E* (in print)
[17] Komatsu N, Kiwata T and Kimura S 2008 *Physica (Amsterdam)* **387A** 2267; 2009 *Physica (Amsterdam)* **388A** 639
[18] Ispolatov I and Karttunen M 2003 *Phys. Rev. E* **68** 036117
[19] Ispolatov I and Karttunen M 2004 *Phys. Rev. E* **70** 026102
[20] Komatsu N and Abe T 2005 *Phys. Rev. E* **72** 021601
[21] Merrall T E C and Henriksen R N 2003 *Astrophys. J.* **595** 43
[22] Chavanis P H 2002 *Astron. Astrophys.* **381** 340
[23] Chavanis P H 2003 *Astron. Astrophys.* **401** 15